Optical Clock Recovery Circuits Using Traveling-Wave Electroabsorption Modulator-Based Ring Oscillators for 3R Regeneration

Zhaoyang Hu, Hsu-Feng Chou, *Student Member, IEEE*, Kohsuke Nishimura, Masashi Usami, John E. Bowers, *Fellow, IEEE*, and Daniel J. Blumenthal, *Fellow, IEEE*

***Abstract*—We describe an optical clock recovery circuit that employs a traveling-wave electroabsorption modulator-based ring oscillator. This approach provides synchronized optical clock and the original optical data signal from the same output at separate wavelengths, eliminating additional timing adjustments for the subsequent nonlinear decision gate for reamplifying, reshaping, and retiming (3R) <<AU: Correct?>> regeneration. Furthermore, additional retiming and lateral reshaping of the original data signal can be realized along with optical clock recovery by synchronized modulation. We present a general model of jitter transfer and locking dynamics for the clock recovery circuit and compare with experimental results. Theoretical results indicate that by using hybrid integration to shorten the cavity length, nanosecond-order locking time can be achieved, which is critical for a variety of applications such as protection switching, optical burst and optical packet switching. Experimental demonstrations of 40-Gb/s optical clock recovery and its application for optical 3R regeneration are presented. The recovered 40-GHz optical clock has 500-fs timing jitter and 8-ps pulsewidth, and within 0.3 μs locking time. 3R experiment is implemented by using the OCR combined with a subsequent regenerative wavelength converter, which provides vertical reshaping function. 3R regeneration is demonstrated with a reduced timing jitter.**

***Index Terms*—Clock recovery, electroabsorption modulator, injection locking, optical packet switching, optical signal processing, regeneration.**

I. Introduction

WAVELENGTH-division multiplexing (WDM) combined with high-speed time division multiplexing allows networks to exploit the terahertz transmission bandwidth of single-mode optical fiber and increase the scalability of all-optical networks [1]. While single-wavelength bit rates have been pushed to 40 Gb/s using electronic time-division multiplexing (ETDM) [2], even greater capacities can be reached with techniques like optical time-division multiplexing (OTDM) for 160 Gb/s and faster [3]. However, the increase in the channel bit rate results in an increase in transmission impairments stemming from fiber chromatic dispersion, fiber nonlinear effects, noise accumulation, crosstalk, and jitter [4] that require reamplifying, reshaping, and retiming (3R) regeneration to be employed [5], [6].

Optical 3R regenerators are of great importance, since the optical signal does not have to be converted to an electrical signal and techniques may be employed that scale to bit rate out of the reach of current electronics. In order to retime and reshape return-to-zero (RZ) signals, clock recovery is performed first to extract the synchronization with a reduced jitter, which is often realized with the aid of electronics. The recovered electrical clock then drives a RZ pulse source to generate optical pulses that implements retiming and lateral reshaping functions. Finally, the generated optical pulses are gated by the original data through a nonlinear decision gate, such as an optical wavelength converter, which provides vertical reshaping. Thus, 3R regenerated data at another wavelength is obtained. Optical wavelength converters in particular are a promising candidate for optical 3R regeneration, since reshaped and retimed data can be copied from one wavelength to another to support switching and routing functions [5]–[7].

To date, optical clock recovery (OCR) circuits based on an electrooptical phase-locked loop (PLL) have been proposed and demonstrated [8]. Although these approaches resulted in a high quality recovered clock, a more compact solution is preferred for practical use. Self-pulsating distributed feedback (DFB) lasers have been applied for OCR [9], but beating between two modes usually results in sinusoidal-like optical clocks. Injection-locked optoelectronic oscillator-based OCR was also demonstrated with high spectral purity, but it requires a relatively more complicated configuration that involves conversion between optical and electrical signals with a photodetector and the feedback of the electrical signal to an electrooptical modulator [10]–[12].

In this paper, we describe a technique to extract the clock from an optical data signal and copy the clock onto a new wavelength while preserving or lateral reshaping the data signal on the original wavelength. The results described here are different from what has been reported before in that the technique incorporates essential functionalities of optical clock recovery, optical pulse generation, and data lateral reshaping within a traveling-wave electroabsorption modulator (TW-EAM)-based ring oscillator. This technique has been shown to operate at 40 Gb/s [13]. The output optical clock and data signal can then be used with a subsequent wavelength converter to realize 3R regeneration.

Manuscript received August 12, 2004; revised January 19, 2005. This work was supported in part by KDDI under Grant 442530-59406 and the State of California under UCDiscovery Grant 597095-19929 **<<AU: OK?>>**.

Z. Hu, H.-F. Chou, J. E. Bowers and D. J. Blumenthal are with Department of Electrical and Computer Engineering, University of California, Santa Barbara (e-mail: huby@ece.ucsb.edu).

K. Nishimura and M. Usami are with KDDI R&D Laboratories Inc., Saitama 356-8502, Japan.

Digital Object Identifier 10.1109/JSTQE.2005.845609

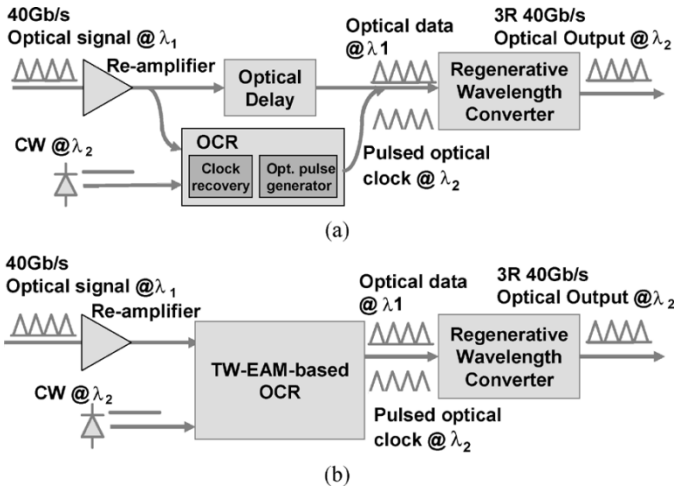

Fig. 1. (a) Conventional optical 3R architecture. (b) New 3R architecture using a TW-EAM-based OCR.

The main advantages of this approach is its simple configuration, the potential monolithic integration, and single input/output fiber coupling for the WDM output of optical data signal and recovered pulsed optical clocks. We first, in Section II, describe the TW-EAM-based ring oscillator and identify its physical basis for OCR operation. In Section III, we formulate the model for the detailed characterization of the timing extraction process and the phase dynamic evolution. The model yields quantitative predictions for the locking range, the jitter transfer of the recovered clock, and the locking time. In Section IV, we describe a series of experiments and then compare them with the theoretical calculations. We also experimentally demonstrate the TW-EAM-based OCR for 40-Gb/s optical clock recovery and its application for optical 3R regeneration. Our conclusions are drawn from the analysis and the experimental results in Section V.

II. Operating Principle

The traditional approach to optical 3R regenerative wavelength conversion is illustrated in Fig. 1(a). A degraded RZ input signal is optically reamplified and then split to an OCR circuit. The OCR includes an optical pulse generator driven by the recovered clock to generate an RZ optical clock pulse train. Subsequently, the recovered pulsed clock enters a regenerative wavelength converter along with the appropriately delayed optical data signal. The wavelength converter essentially uses the data as a control signal to gate the recovered RZ optical clock to perform 3R regeneration.

In this paper, we describe a different approach for optical 3R regeneration as shown in Fig. 1(b). In this approach the TW-EAM-based OCR is injection locked to the clock frequency and imprints only the clock tone from the input data signal (λ_1) onto a new wavelength (λ_2). The data signal is remained or lateral reshaped on the original wavelength; hence, the recovered clock and the data signal from the same output can be directly injected into a wavelength converter to complete 3R regeneration without an optical delay or a separate optical pulse generator.

This work builds on a 40-Gb/s OCR using direct optical injection locking of a TW-EAM-based ring oscillator reported in [13]. The OCR, shown schematically in Fig. 2(a), uses a

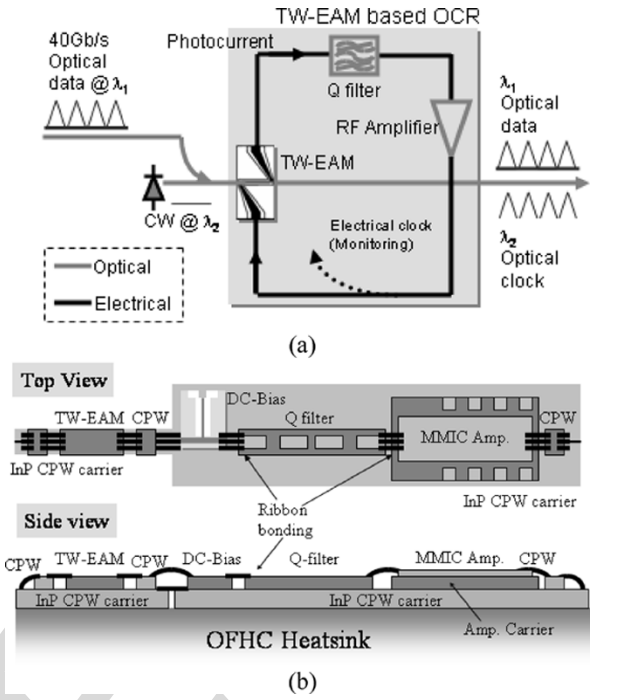

Fig. 2. (a) Scheme of the TW-EAM-based OCR (b) Its hybrid integration configuration.

TW-EAM, an RF Q filter, and an RF amplifier to construct a 40-GHz self-oscillating ring oscillator. The TW-EAM works simultaneously as a photodetector by using photocurrent from the upper electrical port and a pulsed optical clock generator by applying the recovered electrical clock on the lower electrical port to modulate the continuous-wave (CW) ***<<AU: Correct?>>*** light at another wavelength. The modulation effect of the recovered electrical clock performs retiming and lateral reshaping of input optical RZ signal due to narrow synchronized TW-EAM's switch window, which can be used as a stand-alone reshaping–retiming (2R) regenerator [14]. The lateral reshaping implementation comes from the nonlinear transfer function of the TW-EAM that converts applied recovered electrical clock with sinusoidal voltage drive into small duty-cycle time switch windows. Thus, the input optical RZ signal is carved or remained depending on its pulsewidth larger or smaller than the switch window. Furthermore, if using cross-absorption modulation (XAM) in the TW-EAM to implement wavelength conversion, 3R regeneration could be achieved within the same OCR circuit. However, slow carrier recovery in the TW-EAM limits its application of 40-Gb/s wavelength conversion. In the following 40-Gb/s OCR experiments, relatively low input signal power was employed and no significant data transfer to CW light was observed.

When the input optical RZ signal contains a frequency within the OCR's locking range, the OCR can be injection locked. Traditionally, this type of circuit requires an external phase shifter. However, the loop phase of the OCR can be tuned by adjusting the bias voltage of the TW-EAM due to the TW-EAM's nonlinear electroabsorption process [13]. In order to decrease the OCR's locking time, the buildup time of the ring oscillator needs to be reduced, which is related to its physical loop length. This can be done by hybrid or monolithic integration of the electrical circuit elements with the TW-EAM. Fig. 2(b)

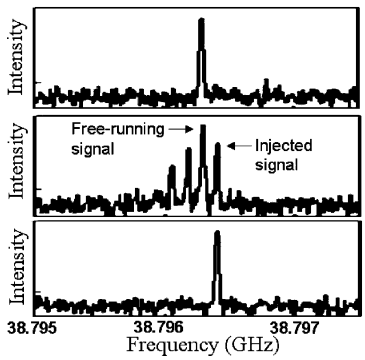

Fig. 3. Injection locking process of the TW-EAM-based OCR with 1-kHz resolution bandwidth. Upper: output RF spectrum of free-running oscillation; Middle: unlocked OCR; Bottom: injection locked OCR.

shows a hybrid integrated realization of the OCR, including a TW-EAM, a dc-bias circuit, a coplanar waveguide Q filter, a 40-GHz narrow-band microwave monolithic IC (MMIC) amplifier interconnected by several coplanar waveguide (CPW) lines, and bonding ribbons [15].

The injection-locking process is shown in Fig. 3 with an applied 40-Gb/s OTDM signal at the input. Without the 40-Gb/s signal, the oscillator free-runs at around 40 GHz, shown as the upper waveform in Fig. 3. When the 40-Gb/s OTDM signal is injected at the edge of the lock-range, both the clock component of the injected signal and the free-running mode exist in the oscillator, along with several other peaks generated by the nonlinear mixing process shown as the middle waveform in Fig. 3. When input signal frequency is within the lock-range, the oscillator-based OCR is injection locked at clock frequency shown as the bottom trace.

III. Theory

A. TW-EAM-Based Ring Oscillator

Like other oscillators, the oscillation of a TW-EAM-based ring oscillator, shown in Fig. 2(a), starts from a noise transient, such as thermal noise and shot noise. After multiple recirculations, free-running oscillation is built up. A Q filter is employed in the loop to select desired modes from equally spaced oscillation modes of the oscillator. Through adjusting gain or loss, only one oscillation mode at frequency $f_{\rm osc}$ is allowed to have unit gain so that stable oscillation is obtained. The noise component at $f_{\rm osc}$ is given

$$V_0(t) = V_n \exp(-i2\pi f_{\rm osc} t) \tag{1}$$

where V_n is its noise amplitude. The noise component of (1) travels around the loop, and the summation of all circulating fields

$$V_{\rm osc}(t) = V_n \sum_{m=0}^{\infty} g^m F_{\rm osc}^m \exp(-i2\pi f_{\rm osc}(t+m\tau)) \tag{2}$$

where g and $F_{\rm osc}$ are the loop voltage gain and the transmission of the Q filter at frequency $f_{\rm osc}$, respectively; τ is the time delay resulting from the physical length of the oscillator; and m is the number of times the field has circulated around the loop, with $V_{m=0}(t) = V_0(t)$. The phase-matching condition requires the satisfaction of the following relationship:

$$2\pi m f_{\rm osc}\tau = 2k\pi, \quad k = 0, 1, 2, \ldots \tag{3}$$

where k is an integer. Therefore, the corresponding RF power of the free-running oscillation signal is

$$P_{\rm osc} = \frac{V_n^2}{2R(1 + g^2 F_{\rm osc}^2 - 2gF_{\rm osc})} \tag{4}$$

where R is the load impedance of the TW-EAM.

B. Jitter Transfer Function

In this section, we consider the jitter transfer function of the injection-locked oscillator for OCR operation. Each oscillator has a negative conductance device, a resonator, and complex noise admittance. If the oscillator is injection locked to the external injected signal, the phase relationship between the oscillator and the injected signal can be described as [16], [17]

$$\frac{d\phi}{dt} = 2\pi f_{\rm osc} - \frac{\pi f_{\rm osc}}{Q} B_n(t) - \frac{\pi f_{\rm osc}}{Q}\sqrt{\frac{P_{\rm inj}}{P_{\rm osc}}}\sin(\phi - \psi_{\rm inj}) \tag{5}$$

where ϕ and $\psi_{\rm inj}$ are the instantaneous phases of the free-running oscillator and injected signals, respectively. $P_{\rm inj}$ is the power intensity of the injected signal and Q is the quality factor of the oscillator. $B_n(t)$ is a time-varying noise susceptance, assumed to be an ergodic process.

For a small noise level, (5) is simplified as the following equation and the detailed derivation can be found in [16] and [17]:

$$S_{\delta\phi}(f) = |H_J(f)|^2 \cdot \left(\frac{f}{\Delta f_{\rm lock}}\right)^2 \cdot S_{\delta\phi_0}(f) + |H_J(f)|^2 \cdot S_{\delta\phi_{\rm inj}}(f) \tag{6}$$

where $\Delta f_{3\ \rm dB} = f_{\rm osc}/2Q$ is half the 3-dB bandwidth of the oscillator; $S_{\delta\phi_0}(f)$ is the power spectral density of the oscillator's phase fluctuations in the absence of an injected signal; $S_{\delta\phi_{\rm inj}}(f)$ is the power spectral density of the phase fluctuations of the injected signal; and $H_J(f)$ is the jitter transfer function of the TW-EAM-based oscillator, given by [17], [18]

$$H_J(f) = \frac{1}{1 + i\frac{f}{\Delta f_{\rm lock}}} \tag{7}$$

where $\Delta f_{\rm lock}$ is the locking range, which is defined from the well-known Adler equation [19]

$$\Delta f_{\rm lock} = \sqrt{\frac{P_{\rm inj}}{P_{\rm osc}}}\frac{f_{\rm osc}}{2Q}. \tag{8}$$

Fig. 4 shows the curves of jitter transfer function versus offset frequency from the carrier for several different locking ranges of 1 kHz, 10 kHz, 50 kHz, 500 kHz, and 1 MHz, respectively. It is obvious that the recovered clock follows the input signal's jitter within the locking range and suppresses the jitter outside the locking range. Within the locking range, the capacity of

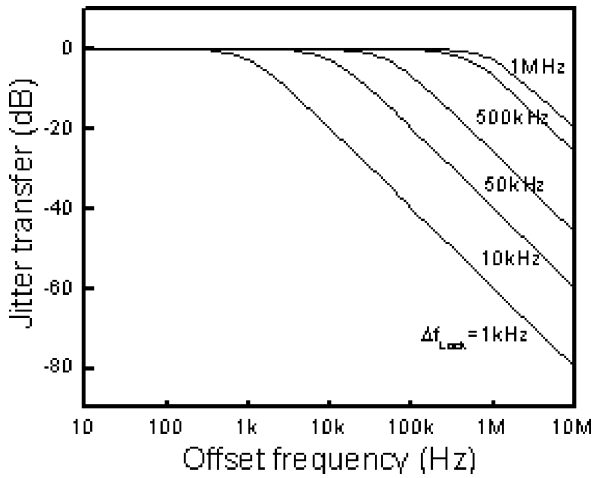

Fig. 4. Simulation of jitter transfer function versus offset frequency for different locking ranges.

the oscillator to track the uncertainty in the arrival time of the input signal plays an important role in its suitability for assuring proper timing. Outside the locking range, lower timing noise, which is attenuated by 20 dB/decade, is desirable for optical 3R regeneration purposes.

C. Transient Response

The transient response of the oscillator describes its dynamic evolution when the locking signal is injected into the free-running oscillator. Since the first two terms in (5) do not contain phase tracking information, we can neglect them and also set $\psi_{\text{inj}} = 0$

$$\frac{d\phi}{dt} = \frac{\pi f_{\text{osc}}}{Q}\sqrt{\frac{P_{\text{inj}}}{P_{\text{osc}}}}\sin(\phi). \tag{9}$$

By integrating (9) for ϕ assuming an initial phase difference ϕ_0 between the free-running oscillation signal and injected signal

$$\int_{\phi_0}^{\phi}\frac{d\phi}{\sin(\phi)} = \sqrt{\frac{P_{\text{inj}}}{P_{\text{osc}}}}\frac{\pi f_{\text{osc}}}{Q}\int_0^t dt \tag{10}$$

which leads directly to

$$\phi(t) = 2\tan^{-1}\left(\exp\left(-\sqrt{\frac{P_{\text{inj}}}{P_{\text{osc}}}}\frac{\pi f_{\text{osc}}}{2Q}t\right)\tan\frac{\phi_0}{2}\right) \tag{11}$$

where Q can be defined as [20]

$$Q = \frac{f_{\text{osc}}}{\Delta f_{3\text{ dB}}} = 2\pi f_{\text{osc}}\tau^2\frac{P_{\text{osc}}}{\rho G_A^2} \tag{12}$$

where G_A is the RF amplifier's voltage gain and ρ is equivalent input noise density. Fig. 5(a) is a plot of the phase response for different initial phases of ϕ_0 at different injection ratio of $P_{\text{inj}}/P_{\text{osc}}$. The parameters for the simulations are $\phi_0 = 25°$, $-80°$, $P_{\text{inj}}/P_{\text{osc}} = -10$ dB, -20 dB, respectively; $P_{\text{osc}} = 10$ dBm, $\tau = 1$ ns, $G_A^2 = 25$ dB, $\rho = 10^{-17}$ mW/Hz. It is seen that smaller initial phase and stronger injection ratio suggest faster evolution process to the steady state.

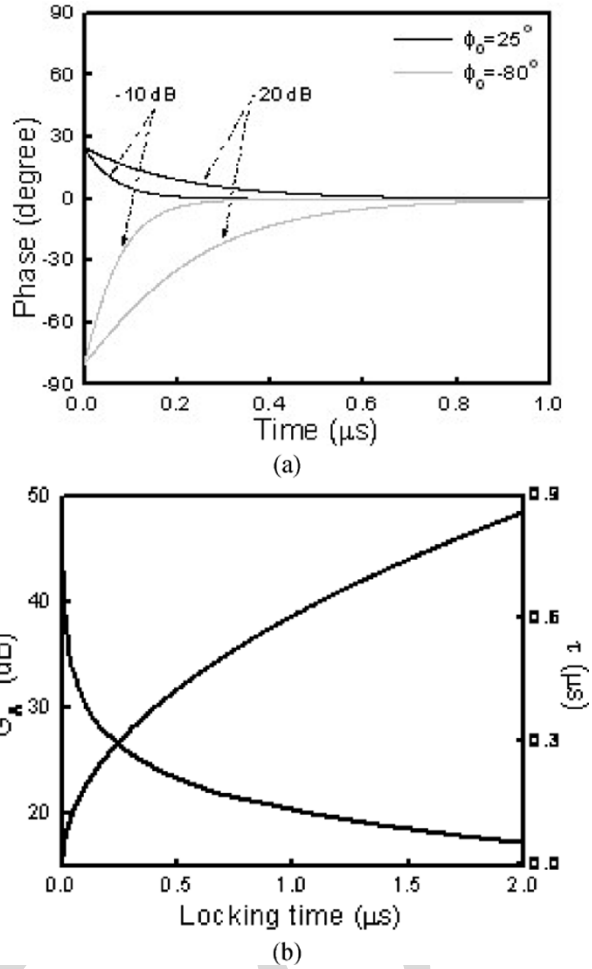

Fig. 5. Simulation of: (a) transient response of the injection locked oscillator and (b) locking time versus the amplifier's gain and the loop delay time.

In addition, increasing the gain of the RF amplifier in the loop can accelerate the oscillator's transient process; and also reducing the loop delay time or loop length can decrease the locking time, shown in Fig. 5(b). It indicates that nanosecond-order locking time could be achieved through increasing the RF amplifier's gain to 35 dB and reducing the loop delay time to 0.01 ns.

IV. Experimental Results

A. TW-EAM-Based Ring Oscillator for 40-Gb/s Optical Clock Recovery Operation

We experimentally investigated the TW-EAM-based ring oscillator for 40-Gb/s optical clock recovery operation. A 10-GHz gain-switched distributed Bragg reflector (DBR) laser was used to generate pulses at 1554 nm (λ_1) and modulated with a $2^{31} - 1$ pseudorandom binary sequence (PRBS) ***<<<AU: Correct?>>>*** pattern by a $LiNbO_3$ modulator and then optically multiplexed to 40-Gb/s OTDM signal. The CW light input for generating recovered optical clock was 6 dBm at 1558 nm (λ_2).

The TW-EAM used in the oscillator has a total extinction ratio of above 30 dB for the transverse magnetic (TM) mode, shown in Fig. 6(a). Details of the TW-EAM have been previously reported in [21]. As a photodetector, its responsivity is 0.4 A/W and its 3-dB bandwidth is 12 GHz, but the rolloff is small. At

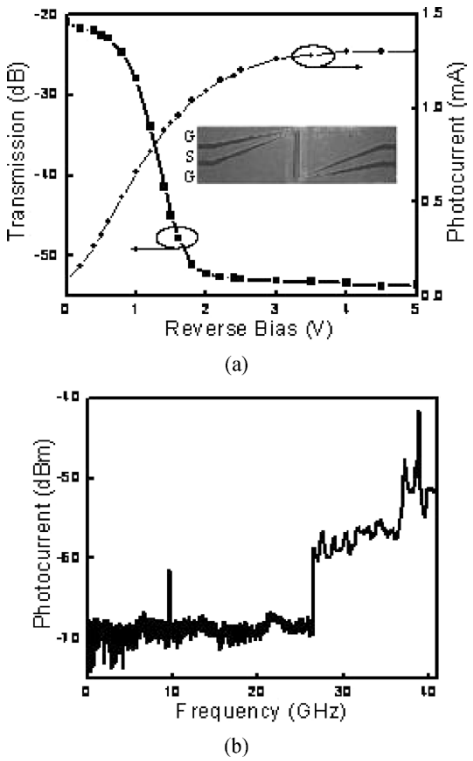

Fig. 6. (a) Transmission and photocurrent curves versus the bias of the TW-EAM. Inset: Layout of the TW-EAM. (b) RF spectrum of the photocurrent with 40-Gb/s OTDM signal injection.

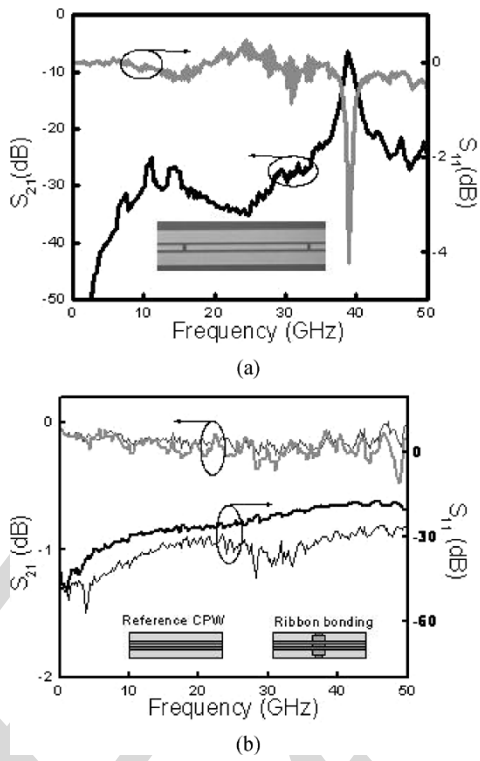

Fig. 7. (a) Frequency response of the Q filter. Inset: Layout of the Q filter. (b) Insertion and reflection losses due to ribbon bonding interconnection (dark curves: ribbon bonding; gray curves: reference CPW lines).

6 dBm input power of 40-Gb/s OTDM signal, the RF spectrum of the TW-EAM's photocurrent is shown in Fig. 6(b) and the 40-GHz tone is −40 dBm. The peak around 10 GHz comes from imperfect OTDM 1 : 4 multiplexing.

The 40-GHz chip coplanar Q filter is realized by creating a capacitively coupled resonant section in the inner conductor. It was fabricated on a semi-insulated InP substrate with a Q factor of about 50 and a sideband suppression ratio of over 20 dB, which is shown in Fig. 7(a). It was bonded to the TW-EAM using 50-μm-wide gold ribbon. As the interconnections, the bonding ribbons' insertion loss is negligibly low compared with the reference CPW lines, but the reflection is 10 dB more at 40 GHz, shown in Fig. 7(b). A 38 GHz-40 GHz RF amplifier is connected to the TW-EAM and Q filter with external RF cables to construct the ring oscillator.

Before injecting a 38.79629-Gb/s OTDM signal, the OCR oscillated at the frequency of 38.7961 GHz that is determined by the peak frequency of Q filter and the loop length (hereafter, we will just use "40-Gb/s OTDM signal" and "40-GHz clock" for simplification). When the OTDM signal is applied, both the clock component and the free-running mode exist in the loop. Through adjusting the TW-EAM's reverse bias voltage to 3 V, the OCR oscillation frequency was tuned close to the input data frequency and its phase was also locked.

The output optical signal from the oscillator was amplified by an erbium-doped fiber amplifier (EDFA) ***<<<AU: Correct?>>>*** and then filtered by a 2.4-nm optical bandpass filter to separate the recovered optical clock at 1558 nm and the OTDM signal at 1554 nm. Fig. 8 shows eye diagrams of the input OTDM signal, output OTDM signal, and recovered optical clock. No significant difference was observed when output data signal was compared with the original input data signal. Fig. 8 also depicts the optical spectrum of simultaneous output of the data signal and the recovered pulsed optical clock at separated wavelengths. The pulsewidth of the recovered optical clock is 8 ps, shown as the inserted autocorrelation curve in Fig. 8. The TW-EAM introduced a 17-dB insertion loss. It can be reduced by carefully matching the mode shapes of the TW-EAM and lensed fibers.

It is important to measure the time required to achieve synchronization of the injection-locked oscillator to an injected signal since the clock locking time will affect system latency. A mixer is used to measure the locking time of the OCR. 40-GHz RF signal electrically multiplexed from 10-GHz RF signal from the transmitter inputs the LO port of the mixer; recovered 40-GHz electrical clock inputs RF port of the mixer. First, optical packets with 1-μs packet length and 1-μs gap enter the oscillator. The output IF signal from the mixer is shown as the lower waveform in Fig. 9(a). The locking time is measured from arrival time of optical packets to that of clock buildup. 0.3-μs locking time was measured in 0.3-m loop length. The oscillator's holding time is also measured, i.e., how long the clock will stay synchronized to data after dropping the injected signal. A 0.4-μs holding time was measured in the OCR. When the packet length and gap of the optical packets were changed to 1 and 0.5 μs, respectively, the output IF signal from the mixer is shown as the lower waveform in Fig. 9(b). It confirms the measurement results of the locking time and holding time.

When we increased the oscillator's loop length from 0.3 to 1.28 m by changing the RF cable lengths, the locking time was increased to 2 μs, shown as the solid scattered dots in Fig. 9(c). The experimental results match (11) and simulation results in

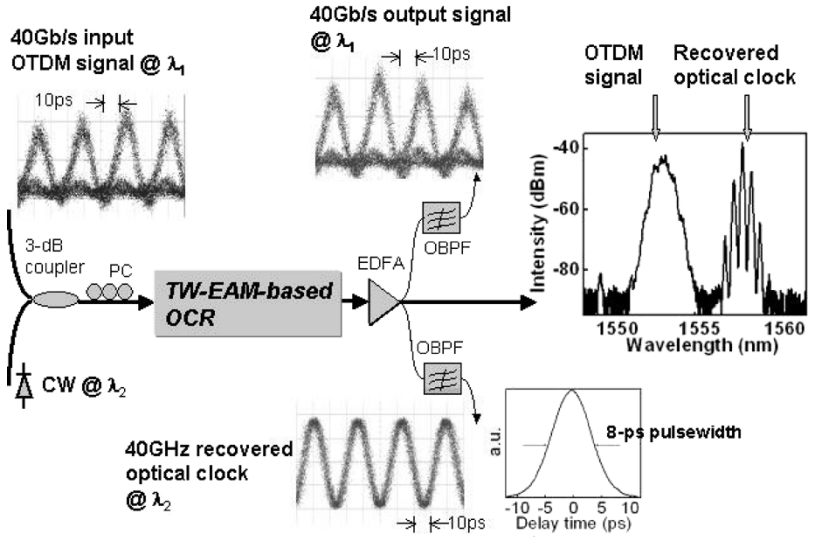

Fig. 8. 40-Gb/s optical clock recovery operation (PC: polarization controller; OBPF: optical bandpass filter).

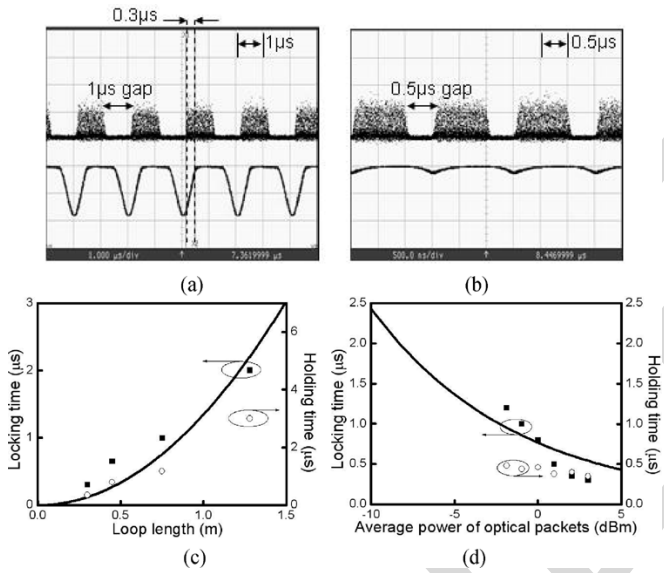

Fig. 9. Input optical packets (upper) and output IF signal from the mixer (lower) with: (a) 1-μs packet length and 1-μs gap; (b) 1-μs packet length and 0.5-μs gap; locking time against (c) the OCR's loop length and (d) average power of input optical packets (solid curves: simulation results; solid and hollow scattered dots: experimental results of locking time and holding time, respectively).

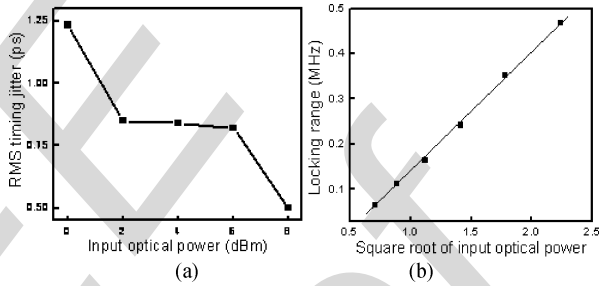

Fig. 10. (a) Timing jitter of recovered optical clock against input optical power. (b) Locking range versus square root of input optical power.

Fig. 5 in Section II. Assuming: 1) 10% power of input optical signal is converted and injected to the OCR; 2) injected signal power is twice the average power due to 50/50 duty cycle of input packets and gaps; and 3) the initial phase is fixed, we approximately simulate the relationship between locking time and the loop length, shown as the solid curve in Fig. 9(c). When the average power of input optical packets was reduced from 3 to -2 dBm, the locking time is increased to 1.2 μs, shown as the solid scattered dots in Fig. 9(d). The simulation results are shown as the solid curve in the figure. We believe the reason why not ***<<<AU: Please provide missing text>>>*** well matched is that the initial phase may be changed in the measurement while assuming fixed in the simulation. We found the holding time is constant at around 0.4 μs for different injection power from -2 to 3 dBm while it increases to 3 μs when the loop length increases to 1.28 m, shown as the hollow scattered dots in Fig. 9(c) and (d), respectively. An oscillator with stronger injection, low losses, and higher gain as well as shorter loop length is desired for fast locking time.

The rms timing jitter of the recovered optical clock (with EDFA amplification) was obtained by integrating its single sideband (SSB) noise spectra from offset frequency of 1 kHz to 10 MHz. At 8 dBm of optical input, its rms timing jitter is 500 fs. When the input power was reduced from 8 to 0 dBm, its timing jitter is increased monotonously, shown in Fig. 10(a). The measured locking range described in Fig. 10(b) shows larger than 400-kHz locking range and a linear relationship dependence on the square root of optical input power, which is consistent with (8).

B. TW-EAM-Based OCR for 3R Regeneration and Its Jitter Transfer Function Measurement

We experimentally investigated the TW-EAM-based OCR for the application of 3R regeneration through feeding its output signals into a subsequent fiber cross-phase modulation (XPM) wavelength converter, shown in Fig. 11. Details of the wavelength converter have been previously reported in [22]. The output signals from the OCR are the original 40-Gb/s data at λ_1 and the recovered 40-GHz optical clock at λ_2, which directly injected into the wavelength converter without any additional timing alignment. Also, no additional optical pulse generator is used in the experiment, since it is already imbedded in the

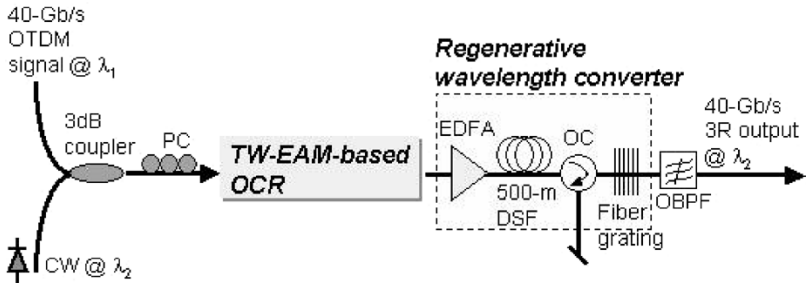

Fig. 11. Optical 3R experiment setup using the TW-EAM-based OCR (PC: polarization controller; OC: optical circulator; OBPF: optical bandpass filter).

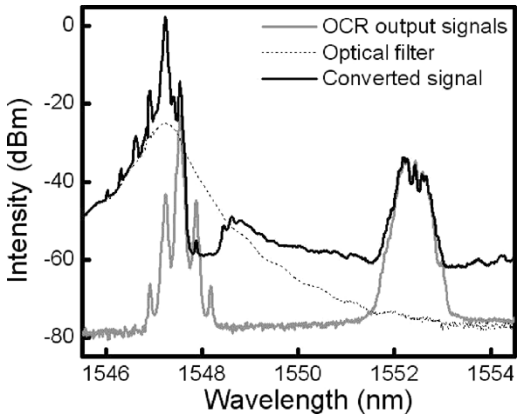

Fig. 12. Optical spectra of output signals from the OCR, optical filter, and wavelength converted signal.

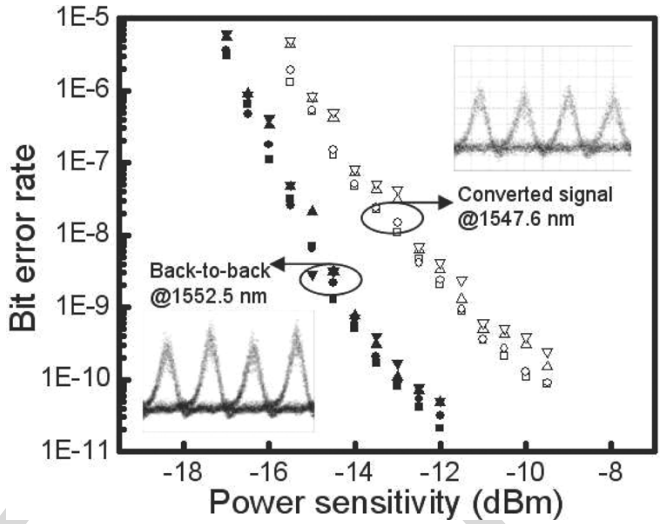

Fig. 13. BER curves and eye diagrams of the 40-Gb/s OTDM input signal and 3R wavelength converted signal.

TW-EAM-based OCR. The fiber XPM wavelength converter has near cosine transfer function and can provide vertical reshaping function [23]. The data pattern is imprinted on the recovered clock pulses through the wavelength converter by the original 40-Gb/s input signal. After filtering out the converted signal at wavelength λ_2, 3R regenerated 40-Gb/s data is achieved.

The wavelength converter is implemented by using the XPM effect in a 500-m-long dispersion shifted fiber (DSF). A 400-mW power level of the input signals is required by the wavelength converter to obtain enough nonlinearity in the DSF fibers. Considering that the fiber XPM wavelength converter is more efficient for down conversion, the wavelength of the CW light input for generating the recovered optical clock is set to 1547.6 nm (λ_2), and the power level is 3 dBm. The wavelength of the 40-Gb/s OTDM signals with $2^{31}-1$ PRBS pattern is 1552.5 nm (λ_1). A 3-dB coupler is used to combine the 40-Gb/s OTDM signal and the CW light together. Then the combined signal is amplified by an EDFA to 12 dBm before entering the OCR. The bias voltage of the TW-EAM is set to 1.06 V considering the output power and modulation efficiency of the TW-EAM. The pulsewidth of the generated optical clock is 10 ps. A shorter pulsewidth can be obtained by increasing the amplitude of the recovered electrical clock applied on the TW-EAM. The converted 40-Gb/s signal from the wavelength converter is filtered out by a 0.6-nm optical bandpass filter.

Fig. 12 depicts the optical spectra of output signals from the OCR, the position of the optical filter, and converted 40-Gb/s signals. The gray curve in Fig. 12 shows the output signals from the OCR. CW light at 1547.6 nm is modulated to generate multipeaks separated at 0.32 nm, and it means a 40-GHz recovered optical clock. After the fiber XPM wavelength converter, the optical spectrum of the recovered optical clock is broadened and one of its sidebands is filtered out as the converted 40-Gb/s signals. The position of the optical filter is shown as the dashed curve in Fig. 12.

Fig. 13 shows the bit error rate (BER) curves and the eye diagrams of the 40-Gb/s back-to-back and 3R wavelength converted signals. The inset waveforms in Fig. 13 show the corresponding eye diagrams. Compared with the back-to-back results, the average power penalty of converted signals for BER $= 10^{-9}$ is 2.7 dB. The power penalty is believed to be partly due to the amplified spontaneous emission (ASE) ***<<<AU: Correct?>>>*** noise of the input optical signal not removed before the OCR so as to be transferred to the subsequent wavelength converter; partly caused by the relatively low power level (-10 dBm) of the OCR's output signals sent to the fiber XPM wavelength converter. The power penalty from the wavelength converter is above 2 dB when the input power level is -10 dBm. Reducing the TW-EAM's loss and using a relative low input power wavelength converter can improve the 3R performance.

Fig. 14(a) depicts the SSB noise spectra of the free-running OCR, input OTDM signal, the recovered optical clock, and the converted signal (with EDFA amplification), which are shown as dashed curve, dotted curve, dark curve, and gray curve, respectively. The SSB noise spectrum of the free-running OCR is obtained by connecting directly to an RF spectrum analyzer while others are obtained via a 50-GHz bandwidth photodiode. The carrier-to-noise at 50-kHz offset is measured to be -71.6,

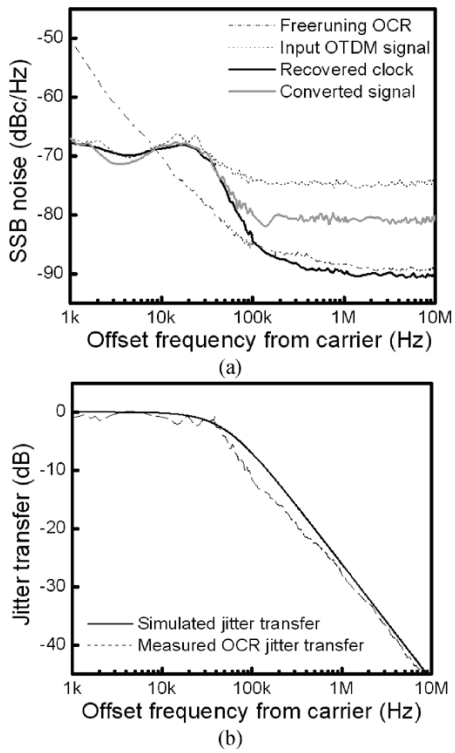

Fig. 14. (a) SSB noise spectra of the free-running OCR, input signal, recovered clock, and wavelength converted signal (resolution bandwidth: 200 Hz). (b) Measured (dashed curve) and calculated (solid curve) jitter transfer functions of the OCR.

-75.5, and -74.6 dBc/Hz for the input OTDM signal, the recovered optical clock, and the converted signal, respectively. Through integrating the noise spectra from offset frequency of 1 kHz to 10 MHz, the rms timing jitters for the input signal, recovered clock, and converted signal are 871, 425, and 537 fs, respectively. The OCR locks to the line-rate frequency while suppressing other frequency components associated with the input signal, which reduces the timing jitter. From Fig. 14(b), it is obvious that inside the 50-kHz locking range, the jitter of the recovered optical clock follows that of the input signal while attenuated by 20-dB/decade outside the locking range, which agrees with the tendency of calculated jitter transfer function shown as the solid curve in Fig. 14(b).

V. Conclusion

We have introduced a compact TW-EAM-based ring oscillator for 40-Gb/s optical clock recovery and its application for optical 3R regeneration. We have presented the general model to analyze the jitter transfer and the locking dynamics of the OCR. We simulated performance characteristics such as the jitter transfer function, locking range, and locking time and confirm the simulation results in a series of experiments. The recovered 40-GHz optical clock has 500-fs rms timing jitter, 8-ps pulsewidth, and 400-kHz locking range. The signals from the same output port of the OCR, i.e., the data signal and recovered optical clock, are directly injected into a subsequent wavelength converter for 3R regeneration without any additional timing adjustment or optical pulse generator. Compared to the input 40-Gb/s RZ signal, 3R wavelength conversion results show reduced timing jitter due to the spectrum purifying effect of the TW-EAM-based OCR. The recovered optical clock from the oscillator can track the timing of input signal inside the locking range while reducing the jitter by 20-dB/decade outside the locking range, which is desirable for optical 3R regeneration application. The transient response analysis and experimental results show that increasing injection power, enhancing the gain of the RF amplifier, and reducing loop length can decrease the locking time. The proposed compact structure consisting of a TW-EAM, a coplanar Q filter, and an RF amplifier is promising for fast OCR provided that monolithic integration is realized to minimize the loop length and hence minimize the corresponding capture time for synchronization.

References

[1] N. S. Bergano and C. R. Davidson, "Wavelength division multiplexing in long-haul transmission systems," *J. Lightwave Technol.*, vol. 14, no. 6, pp. 1299–1309, Jun. 1996.

[2] P. M. Krummrich, E. Gottwald, C.-J. Weiske, A. Schopflin, I. Kotten, and B. Lankl, "40 Gbit/s ETDM for long haul WDM transmission," in *Proc. 15th Annu. Meeting Lasers and Electro-Optics Society (LEOS 2002)*, pp. 71–72.

[3] U. Feiste, R. Ludwig, C. Schubert, J. Berger, C. Schmidt, and H. G. Weber, "160 Gbit/s transmission over 116 km field-installed fiber using 160 Gbit/s OTDM and 40 Gbit/s ETDM," in *Conf. Optical Fiber Communication (OFC)*, vol. 4, 2001, pp. ThF3-1–ThF3-3.

[4] M. Saruwatari, "All-optical signal processing for terabit/second optical transmission," *IEEE J. Sel. Topics Quantum Electron.*, vol. 6, no. 6, pp. 1363–1374, Nov./Dec. 2000.

[5] O. Leclerc, B. Lavigne, E. Balmefrezol, P. Brindel, L. Pierre, D. Rouvillain, and F. Seguineau, "Optical regeneration at 40 Gb/s and beyond," *J. Lightwave Technol.*, vol. 21, no. 11, pp. 2779–2790, Nov. 2003.

[6] T. Otani, T. Miyazaki, and S. Yamamoto, "40-Gb/s optical 3R regenerator using electroabsorption modulators for optical networks," *J. Lightwave Technol.*, vol. 20, no. 2, pp. 195–200, Feb. 2002.

[7] K. Nishimura, M. Tsurusawa, and M. Usami, "Optical 3R regeneration with single InGaAsP/InP electroabsorption modulator," in *Indium Phosphide and Related Materials (IPRM) Conf.*, 2002, pp. 677–680.

[8] D. T. K. Tong, K.-L. Deng, B. Mikkelsen, G. Raybon, K. F. Dreyer, and J. E. Johnson, "160 Gbit/s clock recovery using electroabsorption modulator-based phased-locked loop," *Electron. Lett.*, vol. 36, pp. 1951–1952, 2001.

[9] C. Bornholdt, B. Sartorius, S. Schelhase, M. Möhrle, and S. Bauer, "Self-pulsating DFB-laser for all-optical clock recovery at 40 Gb/s," *Electron. Lett.*, vol. 36, pp. 327–328, 2000.

[10] X. S. Yao and G. Lutes, "A high-speed photonic clock and carrier recovery device," *IEEE Photon. Technol. Lett.*, vol. 8, no. 5, pp. 688–691, May 1996.

[11] L. Huo, Y. Dong, C. Lou, and Y. Gao, "Clock extraction using an optoelectronic oscillator from high-speed NRZ signal and NRZ-to-RZ format transformation," *IEEE Photon. Technol. Lett.*, vol. 15, no. 7, pp. 981–983, Jul. 2003.

[12] J. Lasri, P. Devgan, R. Tang, and P. Kumar, "Ultralow timing jitter 40-Gb/s clock recovery using a self-starting optoelectronic oscillator," *IEEE Photon. Technol. Lett.*, vol. 16, no. 1, pp. 263–265, 2004.

[13] Z. Hu, H.-F. Chou, J. E. Bowers, and D. J. Blumenthal, "40-Gb/s optical clock recovery using a travelling-wave electroabsorption modulator-based ring oscillator," *IEEE Photon. Technol. Lett.*, vol. 16, no. 5, pp. 1376–1378, May 2004.

[14] Z. Hu, K. Nishimura, H. Chou, L. Rau, M. Usami, J. E. Bowers, and D. J. Blumenthal, "40 Gb/s optical packet clock recovery using a traveling-wave electroabsorption modulator-based ring oscillator," in *Proc. Eur. Conf. Optical Communication (ECOC)*, 2004, pp. 436–437.

[15] Z. Hu, B. Liu, X. Yan, J. E. Bowers, and D. J. Blumenthal, "All-optical 40 Gb/s cross-wavelength transferred clock recovery for 3R wavelength conversion using a traveling-wave electroabsorption modulator-based resonant cavity," in *Proc. Conf. Optical Fiber Communications (OFC)*, 2004, pp. WD3-1–WD3-3.

[16] H. C. Chang, X. Cao, U. K. U. K. Mishra, and R. A. York, "Phase noise in coupled oscillators: Theory and experiment," *IEEE Trans. Microw. Theory Tech.*, vol. 45, no. 5, pp. 604–615, May 1997.

[17] J. Lasri and G. Eisenstein, "Phase dynamics of a timing extraction system based on an optically injection-locked self-oscillating bipolar heterojunction phototransisitor," *J. Lightwave Tech.*, vol. 20, no. 11, pp. 1924–1932, Nov. 2002.

[18] P. Trischitta and E. Varma, *Jitter in Digital Transmission Systems*. Norwood, MA: Artech House, 1989, ch. 2.
[19] R. Adler, "A study of locking phenomenon in oscillators," *Proc. IEEE*, vol. 61, no. 10, pp. 1380–1385, Oct. 1973.
[20] X. S. Yao and L. Maleki, "Optoelectronic microwave oscillator," *J. Opt. Soc. Amer. B*, vol. 13, pp. 1725–1735, 1996.
[21] Y.-J. Chiu, H.-F. Chou, V. Kaman, P. Abraham, and J. E. Bowers, "High extinction ratio and saturation power traveling-wave electroabsorption modulator," *IEEE Photon. Technol. Lett.*, vol. 14, no. 6, pp. 792–794, Jun. 2002.
[22] B.-E. Olsson, P. Ohlen, L. Rau, and D. J. Blumenthal, "A simple and robust 40-Gb/s wavelength converter using fiber cross-phase modulation and optical filtering," *IEEE Photon. Technol. Lett.*, vol. 12, no. 7, pp. 846–848, Jul. 2000.
[23] P. Ohlen, B.-E. Olsson, and D. J. Blumenthal, "Wavelength dependence and power requirements of a wavelength converter based on XPM in a dispersion-shifted optical fiber," *IEEE Photon. Technol. Lett.*, vol. 12, no. 5, pp. 522–524, May 2000.

Zhaoyang Hu was born in China in 1970. He received the Ph.D. degree from Tsinghua University, Beijing, China, in 2000.

From August 2000 to July 2001, he was a Postdoctoral Research Associate in the Photonic Switching and Integrated Optoelectronics Laboratory, University of Maryland, College Park (UMCP), where he investigated high-power semiconductor lasers and advanced packaging on the silicon optical bench. Since then, he has been a Postdoctoral Researcher in the Optical Communications and Photonics Networks Group, University of California, Santa Barbara (UCSB). He has published more than 30 archival journal papers and presented more than ten conference talks. His current research interests include optoelectronics integration and packaging, optical packet routing and switching, and high-speed optical signal processing in semiconductor devices, with emphasis on clock recovery and 3R regeneration.

Dr. Hu is a Member of the Optical Society of America.

Hsu-Feng Chou (S'01) received the B.S. degree in physics and the M.S. degree in electrooptical engineering from National Taiwan University (NTU), Taipei, Taiwan, in 1996 and 1998, respectively. Since 2000, he has been working toward the Ph.D. degree at the University of California, Santa Barbara (UCSB).

While at NTU, his research focused on quasi-phase-matched second-order nonlinear effects, including numerical simulation and device fabrication. His current research at UCSB involves optoelectronic subsystems based on traveling-wave electroabsorption modulators for optical signal processing in optical time-division multiplexing (OTDM) and wavelength-division multiplexing (WDM) networks, with emphasis on time-domain add–drop multiplexing, demultiplexing, clock recovery, wavelength conversion, and 3R regeneration.

Mr. Chou is a Student Member of the Photonics Society of Chinese-Americans.

Kohsuke Nishimura received the B.S. and M.S. degrees in electrical engineering from Tokyo Institute of Technology, Tokyo, Japan, in 1986 and 1988, respectively.

Since 1988, he has been with KDDI R&D Laboratories, Saitama, Japan, where he has been studying visible light emission materials including II–VI semiconductors and porous silicon. Currently, he is engaged in the research and development of all-optical regeneration, wavelength conversion technologies, and all-optical functional devices for future photonic networks.

Mr. Nishimura is a Member of the Japan Society of Applied Physics (JSAP) and the Institute of Electronics, Information, and Communication Engineers of Japan (IEICE).

Masashi Usami received the B.S., M.S. and Ph.D. degrees in electronic and communication engineering from Waseda University, Tokyo, Japan, in 1981, 1983, and 1992, respectively.

Since 1985, he has been with KDDI R&D Laboratories, Saitama, Japan where he has been studying InGaAsP-InP distributed feedback (DFB) lasers and InGaAs-GaAs high-power lasers. From 1989 to 1990, he was also a Fellow of the Center of Advanced Educational Services, Massachusetts Institute of Technology, Cambridge, where he studied bistability of resonant tunneling diode. Currently, he is engaged in the research and development of all-optical regeneration, wavelength conversion technologies, and all-optical functional devices for future photonic networks.

Dr. Usami is a Member of the Japan Society of Applied Physics (JSAP) and the Institute of Electronics, Information, and Communication Engineers of Japan (IEICE).

John E. Bowers (S'78–M'81–SM'85–F'93) received the M.S. and Ph.D. degrees from Stanford University.

He worked for AT&T Bell Laboratories and Honeywell before joining the University of California, Santa Barbara (UCSB). He is Director of the Multidisciplinary Optical Switching Technology Center (MOST), and a professor in the Department of Electrical Engineering at UCSB. He is also Cofounder of the Center for Entrepreneurship and Engineering Management, and a Cofounder of Terabit Technology and Calient Networks ***<<<AU: Locations?>>>***. He has published six book chapters, 350 journal papers, and 600 conference papers and has received 38 patents. His research interests are primarily concerned with optoelectronic devices and optical networking.

Dr. Bowers is a Fellow of the Optical Society of America and the American Physical Society and a recipient of the IEEE Lasers and Electro-Optics Society (LEOS) William Streifer Award and the South Coast Business and Technology Entrepreneur of the Year Award.

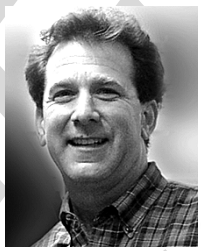

Daniel J. Blumenthal (S'91–M'93–SM'97–F'03) received the B.S.E.E. degree from the University of Rochester, Rochester, NY, in 1981, the M.S.E.E. degree from Columbia University, New York, in 1988, and the Ph.D. degree from the University of Colorado, Boulder, in 1993.

In 1981 he worked at StorageTek, Louisville, CO, and from 1993 to 1997 he was Assistant Professor in the School of Electrical and Computer Engineering, Georgia Institute of Technology, Atlanta. He is currently Professor in the Department of Electrical and Computer Engineering at the University of California, Santa Barbara. He is Principal Investigator for the Defense Advance Research Projects Agency Data in the Optical Domain Network (DOD-N) ***<<<AU: Correct?>>>*** LASOR project and currently serves on the Board of Directors for National LambdaRail (NLR), a national footprint optical network research infrastructure. His research areas are in optical communications, photonic packet switched and all-optical networks, all-optical wavelength conversion, optical subcarrier multiplexing, integrated-optic chip-scale wavelength-division multiplexing (WDM), and nanophotonic technologies. He has authored or coauthored over 160 papers in these and related areas.

Dr. Blumenthal is a Member of the IEEE Lasers and Electro-Optics Society (LEOS) and the Optical Society of America. He is recipient of a 1999 Presidential Early Career Award for Scientists and Engineers (PECASE) from the White House and the Department of Defense, a 1994 National Science Foundation Young Investigator (NYI) Award, and a 1997 Office of Naval Research Young Investigator Program (YIP) Award. He is an Associate Editor for the IEEE PHOTONICS TECHNOLOGY LETTERS and has served as Associate Editor for the IEEE TRANSACTIONS ON COMMUNICATIONS. He was a Guest Editor for the IEEE JOURNAL OF LIGHTWAVE TECHNOLOGY special issue on Photonic Packet Switching Systems (December 1998) and Guest Editor for the IEEE JOURNAL OF SELECTED AREAS IN COMMUNICATIONS special issue on High-Performance Optical/Electronic Switches/Routers for High-Speed Internet. Dr. Blumenthal has served as the General Program Chair for the 2001 Optical Society of America Topical Meeting on Photonics in Switching and as Program Chair for the 1999 Meeting on Photonics in Switching. He has also served on numerous other technical program committees, including the Conference on Optical Fiber Communications (OFC) (1997–2000) and the Conference on Lasers and Electrooptics (CLEO) (1999–2000).